

# Fluorine-Free Poly(ionic Liquid)s Binders for the Aqueous Processing of High-Voltage NMC811 Cathodes

Ana Clara Rolandi, Cristina Pozo-Gonzalo, Iratxe de Meatza, Nerea Casado, David Mecerreyes,\* and Maria Forsyth\*

The use of water-soluble binders enables the transition to more sustainable batteries by the replacement of toxic *N*-methyl-2-pyrrolidone (NMP) by water. Herein, two new fluorine-free poly(ionic liquid)s are proposed as binders for  $\text{LiNi}_{0.8}\text{Mn}_{0.1}\text{Co}_{0.1}\text{O}_2$  (NMC811) cathodes, based on poly(diallyldimethylammonium) (PDADMA) and two-phosphate counter anions, which are recognized as effective corrosion inhibitors and electrolyte additives. Due to their high ionic conductivity ( $10^{-6} \text{ S cm}^{-1}$  at  $25^\circ\text{C}$ ) and ability to prevent degradation of NMC811 particles, the PDADMA phosphate cells are able to achieve a 91% of capacity retention after 90 cycles at 0.5C, similar to the organic fluorinated polyvinylidene fluoride (PVDF) (96%) under the same conditions. However, aqueous sodium carboxymethyl cellulose (Na-CMC) only provides 81% of capacity retention. Among the PDADMA-based binders under study, PDADMA-diethyl phosphate (PDADMA-DEP) delivers the highest discharge capacity ( $101.1 \text{ mAh g}^{-1}$ ) at high C-rate (5C). Degradation of Na-CMC electrodes is observed in postmortem analysis and a notable increase in the charge transfer-resistance. However, the NMC811 particles preserve their spherical shape when PDADMA-phosphates are used as binders, also leading to lower polarization resistances and improved lithium diffusion. In conclusion, PDADMA-phosphates manifest high performance as binders for sustainable NMC811 cathodes, while disposing of fluoropolymers and toxic solvents.

batteries are playing an increasingly significant role in electrical energy storage because of their high specific energy (energy per unit weight) and energy density (energy per unit volume).<sup>[1]</sup> Among several types of lithium batteries, the lithium-ion batteries (LIBs) technology has been used in a wide range of applications since it delivers the best compromise between energy density, power capability, safety, lifetime, and cost.<sup>[2]</sup> LIBs are generally classified according to the atomic structure of their cathode materials including olivine phosphates ( $\text{LiMPO}_4$ ), layered ( $\text{LiMO}_2$ ), or spinel ( $\text{LiM}_2\text{O}_4$ ) oxides, where M represents one or more transition metals. Specifically, NMC811 ( $\text{LiNi}_{0.8}\text{Mn}_{0.1}\text{Co}_{0.1}\text{O}_2$ ) is considered the next-generation cathode active material, due to its low cobalt content, high discharge voltage, and good thermal stability.<sup>[3]</sup>


During the past decades, a great deal of effort has been made to boost the performance of LIBs in order to meet current and future demands. The research was mainly focused on the development of new active materials or electrolytes, but

during the last years, the role of the binder has gained importance. Despite of its low mass contribution with respect to the total electrode composition (2–5 wt%),<sup>[4]</sup> the binder ensures a suitable cohesion giving a homogeneous and well-dispersed slurry that contains all the components of the electrode, acting as a dispersant and thickener.<sup>[5]</sup> Second, the binder penetrates in the surface of the active particles, creating a bonding system

## 1. Introduction

Nowadays, one of the world's most pressing challenges for society is to mitigate the impact of climate change and to create a clean-energy economy. In June 2021, a new European Climate Law established the aim of reaching zero greenhouse gas emissions (GHG) in the European Union by 2050. Lithium

A. C. Rolandi, C. Pozo-Gonzalo, M. Forsyth  
Institute for Frontier Materials  
Deakin University  
Melbourne, Victoria 3125, Australia  
E-mail: maria.forsyth@deakin.edu.au

 The ORCID identification number(s) for the author(s) of this article can be found under <https://doi.org/10.1002/aesr.202300149>.

© 2023 The Authors. Advanced Energy and Sustainability Research published by Wiley-VCH GmbH. This is an open access article under the terms of the Creative Commons Attribution License, which permits use, distribution and reproduction in any medium, provided the original work is properly cited.

DOI: 10.1002/aesr.202300149

A. C. Rolandi, I. de Meatza  
CIDETEC Basque Research and Technology Alliance (BRTA)  
Paseo Miramon 196, 20014 Donostia-San Sebastian, Spain

A. C. Rolandi, N. Casado, D. Mecerreyes, M. Forsyth  
POLYMAT  
University of the Basque Country UPV/EHU  
Avenida Tolosa 72, 20018 Donostia-San Sebastián, Spain  
E-mail: david.mecerreyes@ehu.es

N. Casado, D. Mecerreyes, M. Forsyth  
IKERBASQUE  
Basque Foundation for Science  
48009 Bilbao, Spain

through mechanical interlocking and intermolecular forces.<sup>[6]</sup> For this, the binder needs to have flexible bonds within its structure to stand the constriction and expansion forces of the charge-discharge process. In addition, strong polar groups are desired to maintain effective interfacial interaction with the particles as well as adhesion to the current collector.<sup>[7]</sup> Finally, the binder needs to be thermally and electrochemically stable in the temperature range of electrode processing and within the voltage range of cycling, respectively.<sup>[8]</sup>

Current LIB technologies employ polyvinylidene fluoride (PVDF) as binder, requiring *N*-methyl-2-pyrrolidone (NMP) as solvent for electrode fabrication, which is a tetarogenic and an irritating compound. This raises health concerns during battery manufacturing processes and also environmental processes due to improper NMP waste disposal that can lead to pollution and harm the aquatic ecosystems.<sup>[9–11]</sup> Therefore, an expensive solvent recovery system is required during electrode fabrication to avoid toxic vapors<sup>[12]</sup> and elevated temperatures are also needed for the drying of electrodes due to NMP high boiling point (202 °C). Furthermore, the presence of fluoride compounds hinders the discarding of the battery once used and is a challenge in the LIB recycling process.<sup>[13]</sup> An ecofriendly electrode processing would imply the substitution of NMP by safe solvents such as water. The main drawback of the water processing of high-energy active materials such as NMC811 is the proton exchange with the lithium ions that are present in the particle surface. As consequence of this process called lithium leaching, lithium hydroxide (LiOH) is released and lithium carbonate (Li<sub>2</sub>CO<sub>3</sub>) is formed in the surface of the NMC811 particles, leading to capacity loss and increase in the resistance of the battery.<sup>[14,15]</sup>

An interesting approach to binder formulations is the use of poly(ionic liquids), which contain ionic moieties in the polymer structure and, if chosen carefully, may improve the lithium diffusion and the long-term stability.<sup>[16–22]</sup> This subclass of polyelectrolytes have aroused interest as binder components given the possibility of improving the ionic conduction pathways within the electrode, the possibility of forming strong bonds between the active and conductive material,<sup>[23]</sup> and the flexibility provided by the polymer backbone.<sup>[24]</sup> One of the most studied poly(ionic liquid)s in energy storage applications is based on poly(diallyldimethylammonium) (PDADMA) with different

counteranions. These poly(ionic liquid)s are obtained by anion exchange of the commercially available PDADMA-Cl that comes with chloride (Cl<sup>-</sup>) as counteranion. Ha et al. proved PDADMA-TFSI as a stable binder for sodium–oxygen batteries, creating an interface that increased the electrocatalytic activity and thus reducing the overpotential of the oxygen reduction reaction.<sup>[25]</sup> Recently, Vauthier et al.<sup>[26]</sup> used PDADMA with fluorinated anions as binders in NMC532 cathodes, obtaining improved cell performances when compared with PVDF electrodes. Nonetheless, the most typical counteranions (TFSI<sup>-</sup>, BF<sub>4</sub><sup>-</sup>, PF<sub>6</sub><sup>-</sup>) used to replace Cl<sup>-</sup> result are water-insoluble polymers.<sup>[27]</sup>

The main goal of this work is to explore water-soluble alternatives of PDADMA poly(ionic liquid)s and how these affect the electrochemical performance of the battery when incorporated as binders in high-voltage NMC811 cathode formulations. For this, we found water-soluble PDADMA derivatives having counteranions different than Cl<sup>-</sup>, which is also known to be corrosive.<sup>[28]</sup> Thus, two different counteranions were selected: diethyl phosphate (DEP) and dibutyl phosphate (DBP). Phosphate ions, in general, are known to be good corrosion inhibitors<sup>[29]</sup> and have been used as electrolyte additives to improve the formation of the cathode–electrolyte interface (CEI) in the positive electrode.<sup>[30,31]</sup> The performance of PDADMA-DEP and PDADMA-DBP as water-soluble binders for an environmentally friendly fabrication of NMC811 cathodes is investigated in this research work. For the sake of comparison, conventional binders PVDF and Na-CMC are also studied, using NMP and water as solvent for electrode preparation, respectively.

## 2. Results and Discussion

### 2.1. Fluorine-Free Water-Soluble Poly(ionic Liquid) Synthesis and Characterization

Two water-soluble poly(ionic liquid)s have been synthesized by anion-exchange reaction as shown in **Figure 1**. First, PDADMA-OH is obtained from commercially available PDADMA-Cl, using the exchange resin IRN78. Then, PDADMA-OH is mixed with stoichiometric amounts of diethyl hydrogen phosphate (DEP) or dibutyl hydrogen phosphate (DBP), obtaining PDADMA-DEP and PDADMA-DBP poly(ionic liquid)s.

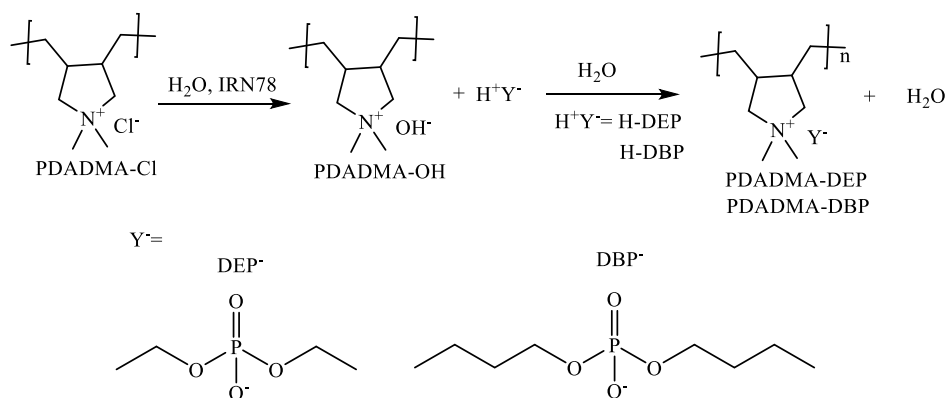


**Figure 1.** Anion exchange reaction for the synthesis of PDADMA-phosphate poly(ionic liquid)s.

The chemical structures of PDADMA-DEP and PDADMA-DBP were confirmed by  $^1\text{H}$  NMR,  $^{31}\text{P}$  NMR, and Fourier-transform infrared (FTIR). **Figure 2a** shows the detailed  $^1\text{H}$  NMR and peak assignment for PDADMA-DEP, which confirm the presence of both the PDADMA and the phosphate

counterion. Furthermore, **Figure 2b** shows both the  $^{31}\text{P}$  NMR of diethyl hydrogen phosphate (H-DEP) at the top and PDADMA-DEP at the bottom. It can be observed that the triplet shifted to higher values of  $\delta$ , confirming the anionic exchange of  $\text{Cl}^-$  by  $\text{DEP}^-$ . As the signal of the H-DEP is not present in the

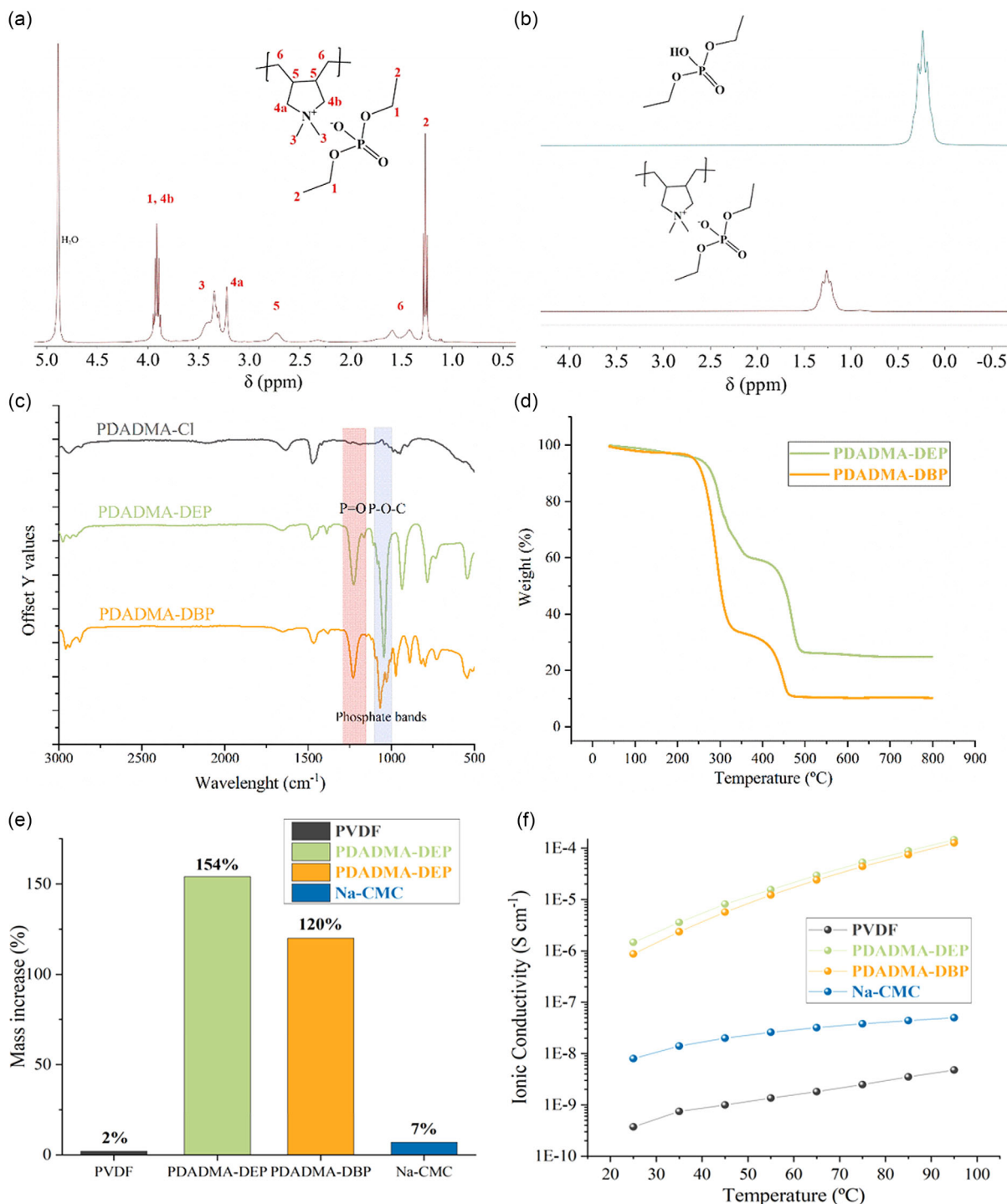


**Figure 2.** a)  $^1\text{H}$  NMR of PDADMA-DEP, b)  $^{31}\text{P}$  NMR of H-DEP and PDADMA-DEP, c) FTIR of PDADMA-Cl, PDADMA-DEP, and PDADMA-DBP, and d) TGA of PDADMA-DEP and PDADMA-DBP from 25 °C to 800 °C at 10 °C min $^{-1}$ . e) Uptake of 1 M LiPF $_6$  in EC:DMC (1:1) + 2% VC electrolyte by the polymer binders after 5 days of immersion in electrolyte, and f) ionic conductivity by EIS measurements between 25 and 95 °C.

PDADMA-DEP, it can be ensured that there is no remaining unreacted H-DEP. The same features are observed for PDADMA-DBP and their  $^1\text{H}$  NMR and  $^{31}\text{P}$  NMR are depicted in Figure S1, Supporting Information. Finally, FTIR measurements were carried out to confirm the chemical structure of the synthesized poly(ionic liquid)s (Figure 2c). When comparing the PDADMA-Cl with the new synthesized poly(ionic liquid)s, new peaks associated with the phosphate counteranion were found. The PDADMA-DEP and PDADMA-DBP spectra presented the characteristic bands of the P=O stretching at  $1230\text{ cm}^{-1}$  and the P–O–C stretching in the vibrational range of  $1060\text{--}1040\text{ cm}^{-1}$ .<sup>[32]</sup>

The drying step of water-processed cathodes is made at  $120\text{ }^\circ\text{C}$  to remove the residual water from the electrode, thus, it is important to evaluate the thermal stability of the PDADMA-phosphates by thermogravimetric analysis (TGA). As depicted in Figure 2d, both show a two-step degradation process with a decomposition temperature of around  $240\text{ }^\circ\text{C}$ , corresponding to 5 wt% of weight loss, confirming the PDADMA-phosphates thermal stability in a wide temperature range. Regarding the PVDF and Na-CMC binders, their thermal stability has been studied by other authors, showing that PVDF starts to degrade at  $420\text{ }^\circ\text{C}$ <sup>[33]</sup> while Na-CMC shows the first step of decomposition at  $150\text{ }^\circ\text{C}$  due to the desorption of water molecules from the structure.<sup>[34]</sup> Therefore, all binders studied in this work are suitable for the temperature range of the LIB electrode processing. Next, the uptake of electrolyte by the polymer binders under study was quantified by undertaking swelling tests. For this, the poly(ionic liquid)s were immersed in the electrolyte solution (1 M  $\text{LiPF}_6$  in EC:DMC (1:1) + 2% VC) for 5 days and the weight increase was monitored (Figure 2e). A larger uptake of electrolyte by the binder will enable a more effective transport of lithium ions through the electrode,<sup>[35]</sup> by creating paths for them to diffuse. The results showed an enhanced uptake of electrolyte for the PDADMA-phosphates, especially for PDADMA-DEP ( $135 \pm 28\%$ ), while PDADMA-DBP resulted in a mass increase of  $120 \pm 8\%$ . As reference values, PVDF and Na-CMC mass only increased by  $2 \pm 1\%$  and  $7 \pm 2\%$ , respectively.

The increased compatibility, and hence solvent uptake of PDADMA-phosphates, can be explained by the presence of polar groups along the structure that increases the affinity with the electrolyte solvents (EC and DMC). Furthermore, the ionic conductivity of PDADMA-based poly(ionic liquid)s was studied by electrochemical impedance spectroscopy (EIS) measurements in the dried state and compared with PVDF and Na-CMC. Figure 2f displays the ionic conductivity results, showing notably higher values at all temperatures for PDADMA-based poly(ionic liquid)s in comparison with PVDF and Na-CMC, since the presence of free anions in the poly(ionic liquid)s increases the ion mobility. Specifically, at the operating temperature ( $25\text{ }^\circ\text{C}$ ), the ionic conductivity for PDADMA-DEP and PDADMA-DBP resulted in  $1.5 \cdot 10^{-6}$  and  $0.87 \cdot 10^{-6}\text{ S cm}^{-1}$ , while Na-CMC and PVDF binders showed lower values,  $8.0 \cdot 10^{-9}$  and  $4.1 \cdot 10^{-10}\text{ S cm}^{-1}$ , respectively.

Finally, binders are required to be electrochemically stable in the potential range of cycling. To check this, cyclic voltammetry (CV) was performed on coin cells without any active material (NMC811). Therefore, working electrodes were prepared with 75 wt% PDADMA-based poly(ionic liquid) and 25 wt% conductive carbon, and lithium metal was used as counter and reference electrodes. The CVs (Figure S2, Supporting Information) probed the electrochemical stability of the PDADMA-phosphate poly(ionic liquid)s, and no significant redox reactions were observed in the range of  $2.0\text{--}5.0\text{ V}$  vs  $\text{Li/Li}^+$ .

## 2.2. Aqueous Processing of NMC811 Cathodes and Electrochemical Performance

Figure 3 outlines the NMC811 cathode processing, including the slurry preparation, casting, and drying of electrodes. As mentioned before, the most frequent binder used is PVDF, which needs to be dissolved in toxic NMP during the slurry mixing. On the other hand, when replacing PVDF by the PDADMA-phosphates poly(ionic liquid)s, not only the cathodes are fluorine free, but also water can be used as solvent. This entails a number

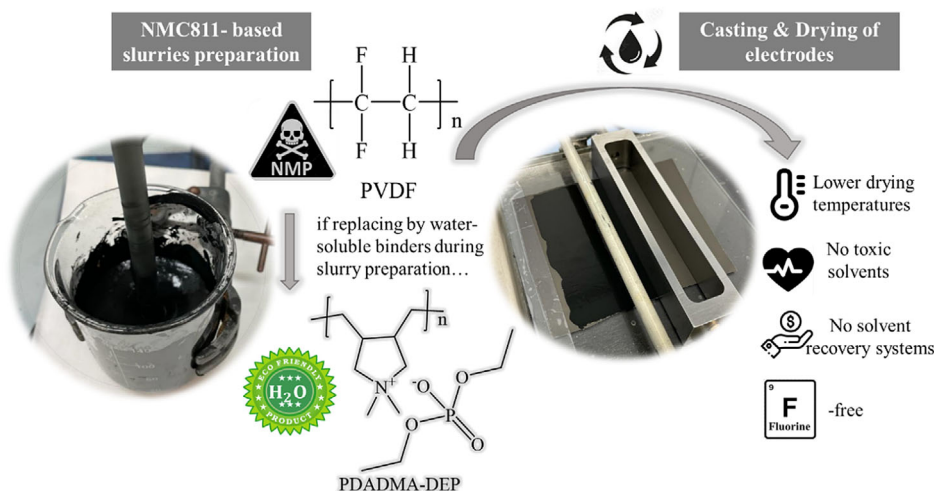


**Figure 3.** Cathode preparation using water-soluble poly(ionic liquid)s-based binders instead of PVDF and its advantages. NMP: N-Methyl-2-pyrrolidone; PVDF: Polyvinylidene fluoride; PDADMA-DEP: Poly(diallyldimethylammonium diethyl phosphate); PDADMA-DBP: Poly(diallyldimethylammonium dibutyl phosphate).

of advantages such as lower drying temperatures, and no need of NMP recovery system, which is translated into lower manufacturing costs.

Therefore, after studying the thermal and electrochemical stability of the water-soluble PDADMA-based poly(ionic liquid)s, slurries were prepared with a composition of 90 wt% NMC811, 5 wt% C45, and 5 wt% poly(ionic liquid)s, using distilled water as solvent. For the sake of comparison, slurries were also prepared using Na-CMC and PVDF as binders. In the latter case, NMP was used for the electrode preparation, since PVDF is not water soluble.

An important function of the binder within the electrode slurry is to disperse the active material and conductive carbon, preventing agglomerations. In this scenario, the viscosity of the slurry and its rheological behavior play an important role. Figure S3, Supporting Information, displays the viscosity of the slurries prepared with different binder compositions as a function of the shear rate. All slurries showed a shear-thinning behavior, where the viscosity decreases with the increase in shear rate. However, a more constant viscosity with increasing shear rate was seen for PDADMA-DEP slurry, suggesting a behavior closer to a Newtonian fluid that presents better dispersion of particles and more stable slurries. As explained in the experimental part, values of the  $n$  factor can be obtained by fitting the curves. These resulted in 0.76, 0.65, 0.56, and 0.44 for slurries with PDADMA-DEP, PDADMA-DBP, Na-CMC, and PVDF as binder, respectively. The closest approximation of PDADMA-DEP to a

Newtonian fluid ( $n = 1$ ) indicates the improved dispersion ability of this binder, followed by PDADMA-DBP.

Afterwards, the NMC811 slurries were casted using the doctor blade technique ( $120 \text{ mm min}^{-1}$ ) onto carbon-coated aluminum current collectors (CC-Al), to avoid the aluminum corrosion as a consequence of the basic pH of the aqueous slurries (measured between 11–12). Then, the electrodes were dried at  $60^\circ\text{C}$  for 1 h. After calendaring to 40% calculated porosity, peeling tests were performed to analyze the effect of changing the binder on the adhesion strength between the active layer and the current collector. The results revealed that PDADMA-DBP electrode presented the highest value ( $20 \pm 1 \text{ N m}^{-1}$ ), followed by PVDF electrode ( $9 \pm 1 \text{ N m}^{-1}$ ), PDADMA-DEP ( $6 \pm 1 \text{ N m}^{-1}$ ), and, finally, Na-CMC ( $4 \pm 1 \text{ N m}^{-1}$ ). The improved adhesion of PDADMA-DBP in comparison with PDADMA-DEP may rely on the larger aliphatic chain of the anion, giving a more robust structure that creates stronger bonds between active particles and with the current collector.

### 2.3. Electrochemical Measurements

The galvanostatic cycling of CR2025 coin cells assembled with the NMC811 cathodes using different binders and graphite anodes is shown in **Figure 4**. The initial charge–discharge cycle curves at 0.1C are displayed in Figure 4a, showing a similar discharge capacity for all cells, around  $200 \text{ mAh g}^{-1}$ , which is the theoretical specific capacity of NMC811.<sup>[36]</sup> In all cases,

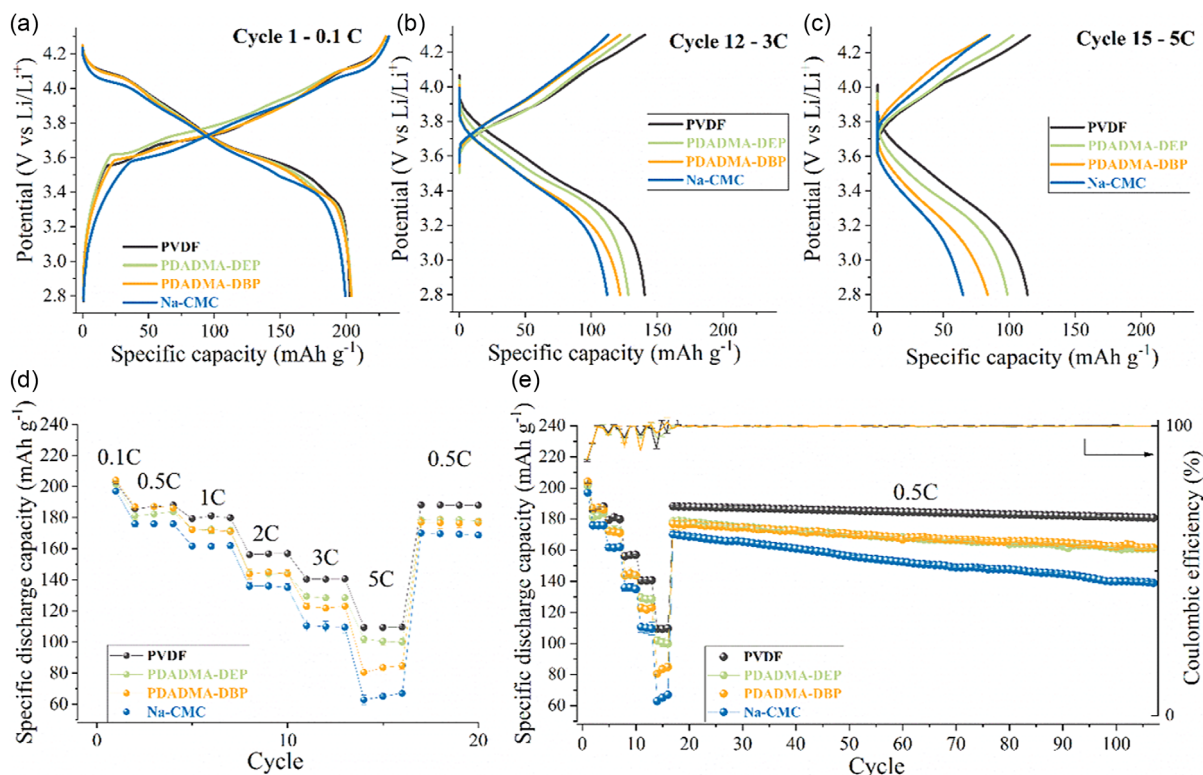


**Figure 4.** Electrochemical performance of NMC811|Graphite coin cells using different binders. Voltage profiles at a) 0.1C, b) 3C, and c) 5C. d) Rate capability performance with 3 cycles at 0.5C, 1C, 2C, 3C, and 5C and e) cycling performance for 90 cycles at 0.5C. Potential range: 2.8–4.3 V (vs.  $V_{\text{cell}}$ ) at  $25^\circ\text{C}$ .

the coulombic efficiency of the initial cycle was close to 88%. As explained by Asenbauer et al.,<sup>[37]</sup> graphite anodes suffer from an irreversible depletion of lithium due to the formation of the solid–electrolyte interphase (SEI). When increasing the C-rate to 3C (Figure 4b) and 5C (Figure 4c), the PDADMA-DEP showed lower overpotentials than PDADMA-DBP and Na-CMC cells, probably due to the higher electrolyte uptake and ionic conductivity. When compared to PVDF, the overpotentials of PDADMA-DEP are higher which is influenced by the damage suffered by the NMC811 active material when exposed to water. Nevertheless, at 5C, the discharge capacities resulted in 109.2, 101.1, 78.9, and 64.5 mAh g<sup>-1</sup> for PVDF, PDADMA-DEP, PDADMA-DBP, and Na-CMC, respectively. Therefore, the PDADMA-DEP binder presented an outstanding high C-rate performance, delivering similar discharge capacity as PVDF-based cathode cells, while disposing the NMP solvent. The larger electrolyte swelling and improved solid particle dispersion ability of the PDADMA-DEP binder may explain its enhanced performance at high C-rates by boosting the lithium transport through the electrode.

Figure 4d summarizes the rate capability of the different binders from 0.1C to 5C. As discussed, the PDADMA-phosphates cells delivered higher discharge capacities at all C-rates than the Na-CMC, but lower than NMP-processed PVDF cells. However, at 0.5C, PDADMA-DBP-based electrode provided the same discharge capacity as PVDF electrode (185.5 mAh g<sup>-1</sup>), closely followed by PDADMA-DEP (182.9 mAh g<sup>-1</sup>), and, finally, Na-CMC (176.1 mAh g<sup>-1</sup>). After the rate capability tests, the current density returned to 0.5C, and the long-term performance was assessed with 90 cycles at 0.5C (Figure 4e). The capacity retentions achieved resulted in 96%, 91%, 91%, and 81% for PVDF, PDADMA-DEP, PDADMA-DBP, and Na-CMC electrodes, respectively. Once again, the PDADMA-phosphates binders were able to improve the cycling performance of the coin cells compared to water-processed Na-CMC, by boosting the lithium transport. Table S1, Supporting Information, summarizes the electrochemical performance of other types of aqueous binders reported in literature for NMC811 cathodes, together with the results of the PDADMA-phosphates binders as comparison. Although there are many factors that can affect the discharge capacities and capacity retention (such as cell type, loading, porosity, electrolyte, cycling protocol, etc), it can be observed that the PDADMA-phosphates binders exhibited outstanding performance as compared to previously reported binders.<sup>[38–43]</sup>

To further understand the reaction kinetics of NMC811 electrodes with the different binders, EIS measurements were carried out from 1 MHz to 1 mHz on pristine and aged electrodes. The pristine electrode corresponds to the condition just assembled and the aged electrode after the galvanostatic cycling. The equivalent circuit used to fit the EIS results is depicted in Figure 5a, as the one employed by Radloff et al. to fit the EIS results of LiNi<sub>0.83</sub>Co<sub>0.12</sub>Mn<sub>0.05</sub>O<sub>2</sub> electrodes.<sup>[44]</sup> The equivalent circuit is composed of an electrolyte resistance ( $R_e$ ), a contact resistance ( $R_{\text{contact}}$ ) between the current collector and the electrode, and a charge transfer resistance ( $R_{\text{ct}}$ ) for the intercalation–deintercalation of lithium ions in the electrode. The two latter processes are represented by double-layer capacitance ( $\text{CPE}_{\text{contact}}$  and  $\text{CPE}_{\text{ct}}$ , respectively). Finally, a Warburg element

( $W_o$ ) is adopted to fit the straight line at low frequencies that represents the lithium diffusion in the electrode bulk.<sup>[45]</sup> The Nyquist plots of the pristine and aged electrodes are presented in Figure 5b,c, respectively, and the fitted data is listed in Table 1.

The electrolyte resistance ( $R_e$ ) in both the pristine and aged condition was alike for all electrodes (between 1Ω and 2Ω), indicating a small contribution of  $R_e$  to the resistance processes inside the cells. In the case of pristine electrodes,  $R_{\text{contact}}$ , corresponding to the first semicircle in the Nyquist plot (Figure 5b), increased from the organic-processed electrode to the water-processed ones that may correspond to the degradation of the NMC811 active material in the aqueous environment. However, between the water-based electrodes, the  $R_{\text{contact}}$  values for the PDADMA-DEP and PDADMA-DBP were lower than for Na-CMC (86.7Ω and 95.5Ω in comparison to 169.3Ω, respectively). This result correlates with the electrochemical performance on the galvanostatic cycling and can be explained by a higher prevention of NMC811 particles degradation by the phosphate species. As reported by Loeffler et al.,<sup>[46]</sup> the deposition of water-insoluble compounds, containing both transition metals and phosphates, protects the high-nickel active material from dissolution. After cycling, the values of  $R_{\text{contact}}$  increased in comparison with the pristine cells, except for the Na-CMC electrode.

As previously mentioned, the  $R_{\text{ct}}$  process is a redox process related to the intercalation–deintercalation of lithium ions between the electrodes. Hence, the diffusion of lithium ions can be boosted by improving the conduction network between active material particles and binder and, therefore, reducing the  $R_{\text{ct}}$  values. As the pristine Nyquist plots only presented one semicircle (Figure 5b), no values of  $R_{\text{ct}}$  were fit for these EIS. However, for the aged electrodes (Figure 5c), the  $R_{\text{ct}}$  resulted in ≈250 Ω for the PDADMA-phosphates and 450 Ω for Na-CMC cells. This difference on the  $R_{\text{ct}}$  values may also explain the enhanced discharge capacity and smaller overpotentials of the PDADMA-phosphates electrodes, since their higher ionic conductivities and uptake of electrolyte may create enhanced pathways for the lithium mobility during the charge and discharge process.

The influence of the binders on the lithium conductivity can be also analyzed from the results acquired by the EIS tests at low frequencies. As explained in the experimental section, by plotting the real part of the total impedance ( $Z'$ ) versus the square root of the angular frequency ( $\omega^{-0.5}$ ), the Warburg factor ( $\sigma$ ) can be obtained from the slope of the curve. In turn, the diffusion coefficient of lithium ions ( $D_{\text{Li}^+}$ ) is inversely proportional to the square of the Warburg factor ( $\sigma$ ).<sup>[35]</sup> The values are listed on Table 1. It can be observed in Figure 5d,e that in both cases the Na-CMC electrodes presented a sharper slope on the  $Z'$  versus  $\omega^{-0.5}$  plots, which indicates larger  $\sigma$  values and, therefore, lower  $D_{\text{Li}^+}$  values. In the pristine cells, Na-CMC almost doubled the value of  $\sigma$ , in comparison with PDADMA-DEP and PDADMA-DBP (344.5, 144.7, and 167.1 Ω s<sup>-0.5</sup>, respectively). In the case of the aged electrodes, Na-CMC presented a value of  $\sigma$  of 8.6 while PDADMA-phosphates and PVDF showed 3.6 and 5.8 Ω s<sup>-0.5</sup>, respectively. The large difference between pristine and aged stages may be because the pristine electrodes have not yet formed all the interfaces, hindering lithium diffusion through the system. Therefore, the PDADMA-phosphates binders present  $D_{\text{Li}^+}$  values of almost one order of magnitude

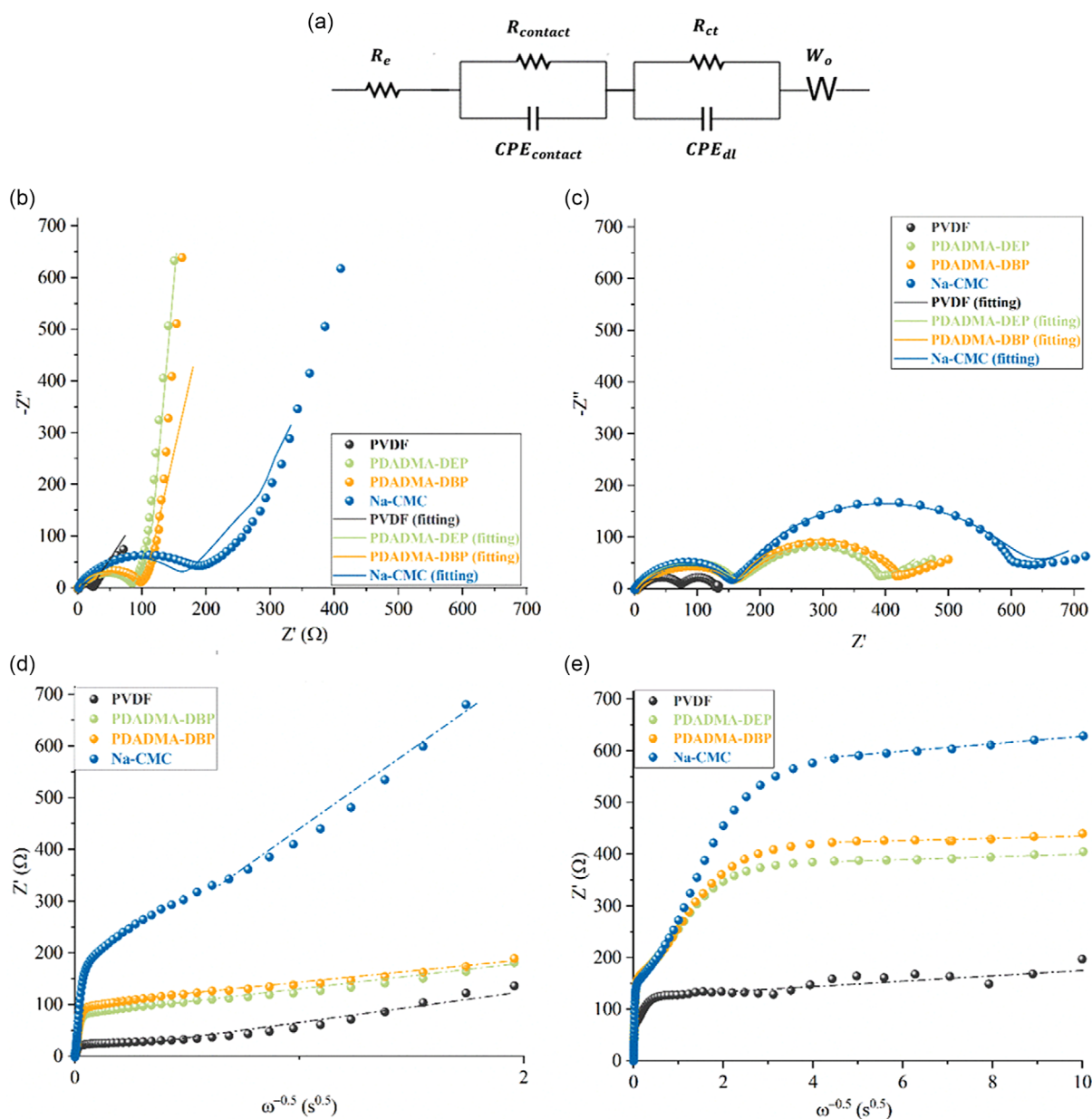


**Figure 5.** a) Equivalent circuit for EIS fitting. Nyquist plot for b) pristine and c) aged NMC811 coin cells.  $Z'$  versus  $\omega^{-0.5}$  of d) pristine and e) aged coin cells.

**Table 1.** Fitted kinetic parameters of NMC811 electrodes obtained by equivalent circuit model.

	$R_e$ [ $\Omega$ ]		$R_{contact}$ [ $\Omega$ ]		$R_{ct}$ [ $\Omega$ ]		$\sigma$ [ $\Omega s^{-0.5}$ ]		$D_{Li^+}$ [ $cm^2 s^{-1}$ ]	
	Pristine	Aged	Pristine	Aged	Pristine	Aged	Pristine	Aged	Pristine	Aged
PVDF	2.3	1.9	28.1	75.1	–	56.4	75.8	5.8	2E-16	3E-14
PDADMA-DEP	1.1	1.9	86.7	155.1	–	234.3	144.7	3.6	4E-17	6E-14
PDADMA-DBP	1.1	2.0	95.5	158.3	–	256.7	167.1	3.6	3E-17	6E-14
Na-CMC	1.6	1.9	168.3	168.1	–	457.1	344.5	8.6	6E-18	1E-14

larger than Na-CMC (Table 1), boosting the lithium mobility and enhancing the electrochemical performance. It is worth mentioning that, in the aged condition, the PDADMA-phosphates-based cells presented slightly higher  $D_{Li^+}$  values than PVDF.

#### 2.4. Postmortem Characterization of the Cathodes

Finally, scanning electron microscope (SEM) measurements were performed on the surface of aged electrodes to further investigate the reason for the different electrochemical behaviors. Low-magnification images of electrodes (**Figure 6a,c,e**) illustrate smooth surfaces for PVDF and PDADMA-phosphates electrodes, unlike the Na-CMC one that presented voids all across the surface (Figure 6g). The holes may hinder the lithium diffusion, explaining the larger  $R_{ct}$  and lower  $D_{Li^+}$  values and, therefore, the poor electrochemical performance. The Na-CMC pristine electrode (Figure S4, Supporting Information) also

presented this morphology, which can be due to heterogeneous water evaporation during the drying step, because of the ineffective dispersion of active and conductive particles, noticed in the rheology results. Figure S4, Supporting Information, also shows that, below the holes in the Na-CMC-based electrode, there is the presence of slurry with active material particles. Furthermore, when increasing the magnification, the PDADMA-phosphates and PVDF-based electrodes depicted spherical active material particles (Figure 6b,d,f). On the other hand, the Na-CMC electrode showed split or cracked NMC811 particles (Figure 6h). Also, a fluffy and porous network can be seen around the active particles in the case of PDADMA-phosphates. By energy dispersive X-ray (EDX) measurements, the presence of the phosphorous element was revealed (Figure S5, Supporting Information), confirming that the PDADMA-phosphates binders form a film around the active particles that prevents the particles degradation and improves the lithium mobility.

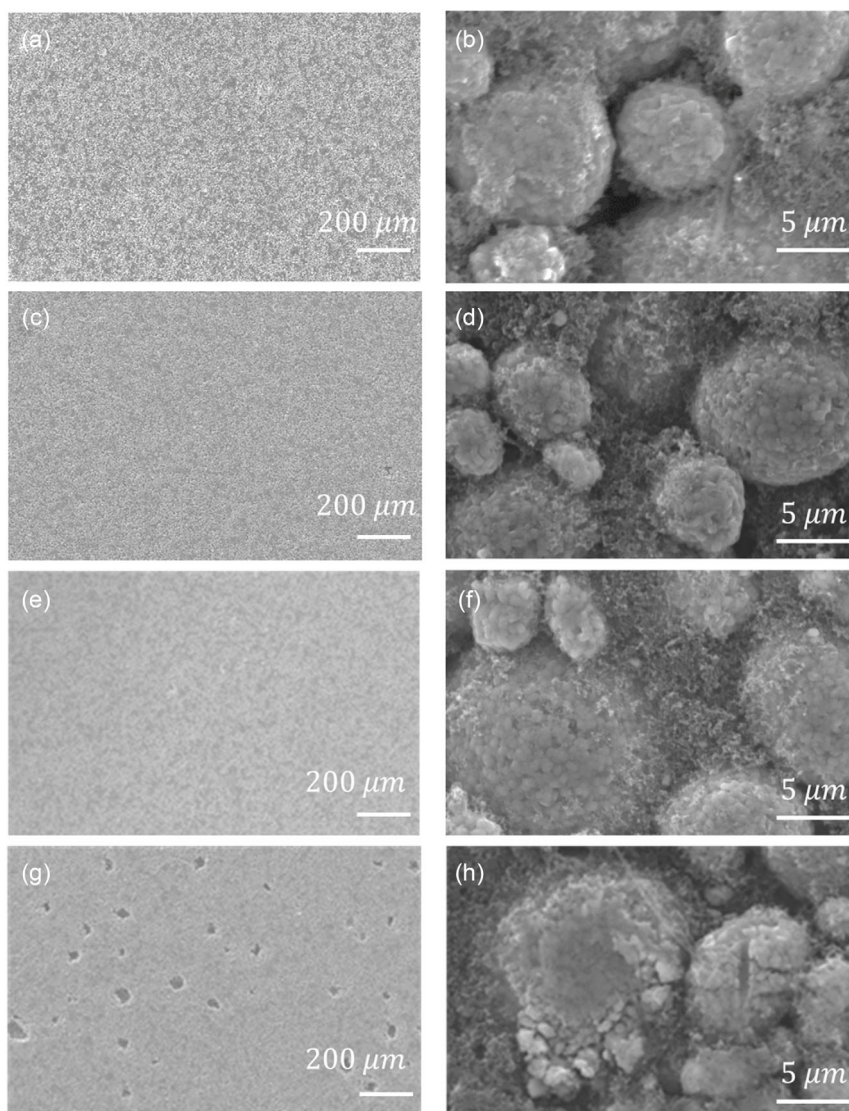


**Figure 6.** SEM images of aged NMC811 electrodes used as binder: a,b) PVDF, c,d) PDADMA-DEP, e,f) PDADMA-DBP, and g,h) Na-CMC.



### 3. Conclusion

In this article we present a new family of poly(ionic liquid) based on poly(diallyldimethylammonium) (PDADMA) and two different phosphate anions in order to obtain two new chemical compounds namely PDADMA-DEP and PDADMA-DBP. One of their main advantages is the water solubility that allows the aqueous processing of battery electrodes, achieving a more sustainable and cost-effective fabrication than traditional organic-processed PVDF. Both poly(ionic liquid)s were thermal and electrochemically stable in the temperature range of processing and in the potential range of cycling, respectively, and presented enhanced ionic conductivities (in the order of  $10^{-6} \text{ S cm}^{-1}$  at  $25^\circ\text{C}$ ) in comparison with traditional binders. Therefore, these poly(ionic liquid)s were applied as water-soluble binders for the aqueous processing of high-energy NMC811 electrodes, achieving homogeneous slurries and, in the case of PDADMA-DBP binder, the adhesion strength resulted higher than for the organic-PVDF electrode. The lithium-ion batteries fabricated with the PDADMA-phosphates-based cathodes showed promising electrochemical performance with high-capacity retention of around 91% after 900 cycles at 0.5C. These results are comparable to the organic solvent NMP-processed cathodes using PVDF as binder and superior to current state-of-the-art water-soluble binder as Na-CMC. This may be explained by the larger ionic conductivity and electrolyte uptake by PDADMA-phosphates binders, which boost the lithium mobility within the electrodes. A lower charge transfer resistance and higher lithium diffusion coefficient was observed by EIS, explaining their improved performance in comparison with Na-CMC. Postmortem microstructural analysis was carried out on the aged electrodes, exhibiting degradation of the active material particles over cycling for the Na-CMC-based electrode, which was not observed in the case of PDADMA-phosphates, where the spherical shape was preserved and no holes were developed in the active layer, while still using water as solvent. In conclusion, these water-soluble PDADMA-phosphates poly(ionic liquid)s are promising binders for an environmentally friendly fabrication of high-energy NMC811 cathodes for lithium-ion batteries.

### 4. Experimental Section

**Materials:** Poly(diallyldimethylammonium chloride) (PDADMA-Cl, 400000-500000 molecular weight, 20 wt% in water, Sigma-Aldrich), diethyl hydrogen phosphate (H-DEP, 95% purity, Sigma-Aldrich), dibutyl hydrogen phosphate (H-DBP, 97% purity, Sigma-Aldrich), Amberlite IRN78 OH hydrogen form (Sigma-Aldrich), poly(vinylidene fluoride) (PVDF, 534000 molecular weight, Sigma-Aldrich), sodium carboxymethyl cellulose (Na-CMC, 250000 molecular weight, Sigma), and 1-methyl-2-pyrrolidone (NMP,  $\geq 99\%$ , Sigma-Aldrich) were used as received.

Conductive carbon C-ENERGY Super C45 (C45) was purchased from Imerys,  $\text{LiNi}_{0.8}\text{Mn}_{0.1}\text{Co}_{0.1}\text{O}_2$  (NMC811, theoretical capacity  $200 \text{ mAh g}^{-1}$ ) was purchased from Targray, and carbon-coated aluminum current collector (CC-Al) from Gelon. Also, for the negative electrode preparation, graphite (Hitachi HE3) and styrene butadiene rubber (SBR, BM451B, Zeon) were used as received.

**Synthesis of Water-Based Poly(ionic liquid)s:** Poly(Diallyldimethylammonium Diethyl Phosphate) (PDADMA-DEP): 12.45 gr of PDADMA-Cl were first diluted in 200 mL of distilled water and passed through a column containing a bed of the exchange resin Amberlite IRN78, collecting PDADMA-OH. Afterwards, 2.5 gr of diethyl hydrogen phosphate (H-DEP) salt were diluted

in 10 mL of distilled water and added drop wise to the aqueous solution of PDADMA-OH. The mixture was stirred at room temperature for at least 1 h. Then, the water was removed by rotary evaporation and dried overnight at  $60^\circ\text{C}$ , obtaining a yellow solid.  $^1\text{H-NMR}$  (400MHz,  $\text{DMSO-d}_6$ ): spectra of PDADMA-DEP displayed characteristic signals of aliphatic chains of DEP at  $\delta$  (ppm): 1.27, 3.92 and the signals corresponding to PDADMA at  $\delta$  (ppm): 1.55, 2.72, 3.22, 3.32, 3.90.

**Synthesis of Water-Based Poly(ionic liquid)s:** Poly(Diallyldimethylammonium Dibutyl Phosphate) (PDADMA-DBP): The same procedure previously described for PDADMA-DEP was used for the synthesis of PDADMA-DBP. In this case, for the 1:1 molar ratio, 3.34 gr of dibutyl hydrogen phosphate (H-DBP) salt were diluted in 10 mL of distilled water and mixed with the same amount of PDADMA-OH solution. The obtained polymer was more sticky than PDADMA-DEP.  $^1\text{H-NMR}$  spectra of PDADMA-DBP displayed characteristic signals of aliphatic chains of DBP at  $\delta$  (ppm): 0.80, 1.30, 1.50, 3.78 and the signals corresponding to PDADMA at  $\delta$  (ppm): 1.50, 2.60, 3.06, 3.15, 3.81.

**Polymer Characterization: Physicochemical Characterization:** The chemical structures of the synthesized poly(ionic liquid)s were confirmed by  $^1\text{H}$  and  $^{31}\text{P}$  nuclear magnetic resonance (NMR) spectroscopy (Bruker Avance III 400 MHz Digital NMR spectrometer) and by FTIR spectroscopy (Nicolet Magna 6700 spectrometer) at room temperature and under air atmosphere. The thermal properties were assessed by TGA using a Q500 analyzer (TA instruments) under nitrogen atmosphere at a rate of  $10^\circ\text{C min}^{-1}$  from  $25^\circ\text{C}$  to  $800^\circ\text{C}$ .

Swelling tests were performed to quantify the uptake of electrolyte by the different binders. For that, the polymers were immersed in the electrolyte for 5 days and then the weight increase was monitored with an analytical balance. The increase in mass percentage was calculated with Equation (1)

$$\text{mass increase (\%)} = \frac{m_1 - m_0}{m_0} * 100 \quad (1)$$

where  $m_0$  and  $m_1$  correspond to the masses before and after immersion.

Ionic conductivity of the PDADMA-based polymers was measured by EIS, using an Autolab 302 N potentiostat galvanostat (Metrohm AG, Herisau, Switzerland) with a temperature control (Microcell HC station). Thin films (1.5 mm) of the samples were previously dried at  $70^\circ\text{C}$  under vacuum overnight and placed between two stainless steel electrodes. The Nyquist plots were obtained by applying a 10 mV perturbation to open circuit in a frequency range from 100 kHz to 1 Hz. The ionic conductivity was estimated by Equation (2)

$$\sigma = \frac{l}{AR} \quad (2)$$

where  $l$  is the film thickness,  $A$  is the electrode area ( $0.5024 \text{ cm}^2$ ), and  $R$  is the film resistance, corresponding to the interception of the impedance curve with the real part of the impedance axis.

**Electrode Preparation:** Cathode slurries of 50 gr of solids were composed by 90 wt% NMC811, 5 wt% carbon black, and 5 wt% binder. In the case of PDADMA-phosphates and Na-CMC binders, water was used as solvent for the electrode preparation. On the other hand, for the PVDF-based electrode, NMP was employed. The first step was to dissolve the binder in the amount of water given by the solid/liquid-ratio (S/L) equal to 1/0.7 for 4 h using mechanical mixing at a high rate to obtain a homogeneous slurry. Then, the slurry was coated on carbon-coated aluminum (CC-Al) current collector using doctor-blade ( $90 \text{ mm min}^{-1}$ ) and metallic stainless steel applicators. The thickness of the coating was adjusted to obtain a loading of  $12 \text{ mg cm}^{-2}$  for all electrodes and dried in a convection oven at  $60^\circ\text{C}$ . By calendaring, the electrodes were densified to obtain a theoretical porosity of 40%, using a roll press (DMP solutions) and a micrometer (Mitutoyo 389-71C) to measure the thickness. Finally, the electrodes were punched with a disk cutter into circular electrodes with a diameter of 16.6 mm. For the graphite anodes, the same procedure of the NMC811 cathodes was followed. The composition was 94 wt% graphite, 2 wt% carbon black, 2 wt% Na-CMC, and 2 wt% SBR latex. The loading of the

anodes was balanced to assemble full cells with a negative-to-positive capacity ratio (N/P) of 1.1 (mass loading of anodes 13.2 mg cm<sup>-2</sup>). In this case, the anodes were cut into circular electrodes of 17.7 mm of diameter.

**Slurry and Electrode Characterization:** Before casting the slurry onto the current collector, rheology measurements were carried out using a rheometer AR 200ex (TA instruments) in parallel plate geometry, with 40 mm diameter and 1 mm gap setting was employed. The measurement was performed at 25 °C between 0.1 and 1000 s<sup>-1</sup> shear rate. The rheology results can be studied with the power-law Equation (3)<sup>[29]</sup>

$$\eta = K\dot{\gamma}^{n-1} \quad (3)$$

where  $\eta$  is the viscosity,  $\dot{\gamma}$  the shear rate,  $K$  is a consistency constant, and  $n$  a factor that quantifies the similarity to a Newtonian fluid (where  $n = 1$ ). Also, the pH of the slurries was measured with pH test strips (Sigma).

Finally, peel tests were carried out to measure the adhesive strength of the electrodes with the different binders. For this, electrodes strips of 2 × 9 cm were stuck onto methacrylate plates with a normalized force and pulled in a 90° angle. The strength value (N m<sup>-1</sup>) was obtained by carrying out the peel test in ambient condition at 20 mm min<sup>-1</sup> crosshead speed (LS1 model, Lloyd Instrument).

**Cell Assembly:** Prior to the assembly of the coin cells, the cathode disks were dried for 16 h at 120 °C under vacuum (10 mbar). The covers of the CR2025 (Hohsen) cells were cleaned with ethanol in an ultrasonic bath for 15 min and then dried at 60 °C for 1 h. Then, the coin cells were assembled using the NMC811 cathodes and graphite anodes in dry-room facilities (dew point of -42 °C). The separators employed were glass fiber type (Whatman GF/A) previously dried at 60 °C and, as electrolyte, 100 μL of 1 mol L<sup>-1</sup> lithium hexafluorophosphate in (1:1 vol%) ethylene carbonate:dimethyl carbonate + 2 wt% vinylene carbonate-99.9% (1 M LiPF<sub>6</sub> in EC:DMC (1:1) + 2% VC, Solvionic).

**Electrochemical Characterization:** CV of the polymers was conducted without the presence of active material. The aim was to detect any redox reaction or irreversible process the polymer undergoes that may contribute to the electrochemical behavior of the battery. To achieve this, the electrodes were prepared only with the polymer binder and conductive carbon (in a 75:25 mass ratio, respectively) and coin cells were assembled with these electrodes using lithium foil as anode and 100 μL 1 M LiPF<sub>6</sub> in EC:DMC (1:1) as electrolyte. After 8 h of stabilization at open-circuit potential, the coin cells were submitted to a CV, using a VMP-3 potentiostat (Biologic Science Instruments) in the range of 2.0–5.0 V (vs. Li/Li<sup>+</sup>) at 0.1 mV s<sup>-1</sup>. The potential was linearly varied with time and the current response was measured.

EIS measurements were performed in pristine and aged (after galvanostatic cycling) electrodes using lithium metal as counterion. In the pristine case, coin cells were assembled using fresh NMC811 electrodes with different binders and lithium metal as anode, and the EIS was performed without any cycling. For the aged measurements, the cells were disassembled after cycling and the recovered NMC811 cathodes were cleaned with dimethyl carbonate (DMC) to remove the electrolyte salts from the surface. After drying for 16 h at 120 °C under vacuum (10 mbar), the electrodes were reassembled with lithium metal as anode to conduct the EIS. In all cases, the separator and electrolyte used were glass fiber type (Whatman GF/A) and 100 μL 1 M LiPF<sub>6</sub> in EC:DMC (1:1) + 2% VC (Solvionic), respectively. Using the Biologic instrument, the EIS was performed using a voltage amplitude of 10 mV and a frequency range varying from 1 MHz to 1 mHz. From the EIS results, by plotting the real part of the total impedance ( $Z'$ ) versus the square root of the angular frequency ( $\omega^{-0.5}$ ), the Warburg factor ( $\sigma$ ) can be obtained following the Randles equation (Equation (4)).<sup>[35]</sup>

$$Z' = R_e + R_{\text{contact}} + \sigma\omega^{-0.5} \quad (4)$$

From the Warburg factor, the lithium-ion diffusion can be found by the Arrhenius equation (Equation (5)).

$$D_{\text{Li}^+} = \frac{R^2 T^2}{2A^2 F^4 C^2 \sigma^2} \quad (5)$$

where  $R$  is the gas constant (8.314 J K<sup>-1</sup> mol<sup>-1</sup>),  $T$  is the absolute temperature,  $A$  is the surface area of the electrode,  $F$  is the Faraday constant (96 500 C mol<sup>-1</sup>), and  $C$  is the molar concentration of lithium ions. The  $A$  and  $C$  factors were complex since the active material was not completely homogeneous and the electrode presented voids and pores. Therefore, in this work, the values for  $A$  (2.16 cm<sup>2</sup>) and  $C$  (1 mol cm<sup>-3</sup>) were assumed constant and the results of  $D_{\text{Li}^+}$  were compared qualitatively.

Galvanostatic charging and discharging cycles were conducted on the NMC811|Graphite coin cells, using a BaSyTec CTS Battery Test System, in a voltage range of 2.8–4.3 V versus  $V_{\text{cell}}$ . After 8 h rest at open-circuit potential, the electrochemical response was tested at different C-rates: C/10, C/2, 1C, 2C, 3C, 5C and, finally, a long-term cycling of 90 cycles at C/2.

**Postmortem Characterization:** After the galvanostatic cycling, the coin cells were disassembled inside a glovebox and the aged cathodes were washed with dimethyl carbonate (DMC) to remove the remaining salts on the surface. SEM images were recorded using a JSM IR 300 series SEM at an accelerating voltage of 2 kV. Also, for the sake of comparison, the SEM images of pristine uncycled electrodes were recorded.

## Supporting Information

Supporting Information is available from the Wiley Online Library or from the author.

## Acknowledgements

This research was supported by the Australian Research Council (ARC) Training Center for Future Energy Storage Technologies (IC180100049) and funded by the Australian Government.

Open access publishing facilitated by Deakin University, as part of the Wiley - Deakin University agreement via the Council of Australian University Librarians.

## Conflict of Interest

The authors declare no conflict of interest.

## Data Availability Statement

The data that support the findings of this study are available on request from the corresponding author. The data are not publicly available due to privacy or ethical restrictions.

## Keywords

aqueous processing, lithium-ion batteries, NMC811 cathodes, poly(ionic liquid)s, water-soluble binders

Received: July 27, 2023

Revised: August 30, 2023

Published online: September 29, 2023

- [1] S. Koochi-Fayegh, M. A. Rosen, *J. Energy Storage* **2020**, *27*, 101047.
- [2] A. Perner, J. Vetter, in *Lithium-Ion Batteries for Hybrid Electric Vehicles and Battery Electric Vehicles*, Elsevier Ltd, Amsterdam **2015**.
- [3] Y. Lv, S. Huang, Y. Zhao, S. Roy, X. Lu, Y. Hou, J. Zhang, *Appl. Energy* **2022**, *305*, 117849.

- [4] J. Li, Z. Wu, Y. Lu, Y. Zhou, Q. Huang, L. Huang, *Adv. Energy Mater.* **2017**, 1701185, 1701185.
- [5] K. Y. Cho, Y. I. Kwon, J. R. Youn, Y. S. Song, *Analyst* **2013**, 138, 2044.
- [6] A. Gören, C. M. Costa, M. M. Silva, S. Lanceros-Méndez, *Composites, Part B Eng.* **2015**, 83, 333.
- [7] X. Zhang, X. Ge, Z. Shen, H. Ma, J. Wang, S. Wang, L. Liu, B. Liu, L. Liu, Y. Zhao, *New J. Chem.* **2021**, 45, 9846.
- [8] S. Ma, M. Jiang, P. Tao, C. Song, J. Wu, J. Wang, T. Deng, W. Shang, *Prog. Nat. Sci.: Mater. Int.* **2018**, 28, 653.
- [9] D. Bresser, D. Buchholz, A. Moretti, A. Varzi, S. Passerini, *Energy Environ. Sci.* **2018**, 11, 3096.
- [10] J. He, H. Zhong, L. Zhang, *J. Appl. Polym. Sci.* **2018**, 135, 12.
- [11] G. T. Pace, H. Wang, J. F. Whitacre, W. Wu, *Nano Select* **2021**, 2, 939.
- [12] N. Lingappan, L. Kong, M. Pecht, *Renewable Sustainable Energy Rev.* **2021**, 147, 111227.
- [13] A. Brilloni, F. Poli, G. E. Spina, C. Samorì, E. Guidi, C. Gualandi, M. Maisuradze, M. Giorgetti, F. Soavi, *Electrochim. Acta* **2022**, 418, 140376.
- [14] H. Buqa, M. Holzapfel, F. Krumeich, C. Veit, P. Novák, *J. Power Sources* **2006**, 161, 617.
- [15] A. Kukay, R. Sahore, A. Parejiya, W. Blake Hawley, J. Li, D. L. Wood, *J. Colloid Interface Sci.* **2021**, 581, 635.
- [16] K. Grygiel, J. S. Lee, K. Sakaushi, M. Antonietti, J. Yuan, *ACS Macro Lett.* **2015**, 4, 1312.
- [17] J. Yuan, S. Prescher, K. Sakaushi, M. Antonietti, *J. Mater. Chem. A* **2015**, 3, 7229.
- [18] J. Von Zamory, M. Bedu, S. Fantini, S. Passerini, E. Paillard, *J. Power Sources* **2013**, 240, 745.
- [19] A. Vizintin, R. Guterman, J. Schmidt, M. Antonietti, R. Dominko, *Chem. Mater.* **2018**, 30, 5444.
- [20] J. S. Lee, K. Sakaushi, M. Antonietti, J. Yuan, *RSC Adv.* **2015**, 5, 85517.
- [21] I. Spanos, S. Neugebauer, R. Guterman, J. Yuan, R. Schlögl, M. Antonietti, *Sustainable Energy Fuels* **2018**, 2, 1446.
- [22] R. Del Olmo, G. Guzmán-González, I. O. Santos-Mendoza, D. Mecerreyes, M. Forsyth, N. Casado, *Batteries Supercaps* **2023**, 6, e202200519.
- [23] Q. Yang, Z. Zhang, X. G. Sun, Y. S. Hu, H. Xing, S. Dai, *Chem. Soc. Rev.* **2018**, 47, 2020.
- [24] G. G. Eshetu, D. Mecerreyes, M. Forsyth, H. Zhang, M. Armand, *Mol. Syst. Des. Eng.* **2019**, 4, 294.
- [25] T. A. Ha, H. Li, X. Wang, L. A. O'Dell, M. Forsyth, C. Pozo-Gonzalo, P. C. Howlett, *ACS Appl. Energy Mater.* **2021**, 4, 434.
- [26] S. Vauthier, M. Alvarez-Tirado, G. Guzmán-González, L. C. Tomé, S. Cotte, L. Castro, A. Guéguen, D. Mecerreyes, N. Casado, *Mater. Today Chem.* **2023**, 27, 101293.
- [27] S. Chauque, F. Y. Oliva, O. R. Cámara, R. M. Torresi, *J. Solid State Electrochem.* **2018**, 22, 3589.
- [28] J. Liao, Z. Ye, *Electrochim. Acta* **2018**, 259, 626.
- [29] Y. Morozov, L. M. Calado, R. A. Shakoor, R. Raj, R. Kahraman, M. G. Taryba, M. F. Montemor, *Corros. Sci.* **2019**, 159, 108128.
- [30] H. Ota, A. Kominato, W. J. Chun, E. Yasukawa, S. Kasuya, *J. Power Sources* **2003**, 119–121, 393.
- [31] S. Tan, Z. Zhang, Y. Li, Y. Li, J. Zheng, Z. Zhou, Y. Yang, *J. Electrochem. Soc.* **2013**, 160, A285.
- [32] J. L. White, *Soil Sci.* **1971**, 112, 22.
- [33] Q. Zhang, Z. Sha, X. Cui, S. Qiu, C. He, J. Zhang, X. Wang, Y. Yang, *Nanotechnol. Rev.* **2021**, 9, 1350.
- [34] M. Ndour, J. P. Bonnet, S. Cavalaglio, T. Lombard, M. Courty, L. Aymard, C. Przybylski, V. Bonnet, *Mater. Adv.* **2022**, 3, 8522.
- [35] M. Ling, J. Qiu, S. Li, C. Yan, M. J. Kiefel, G. Liu, S. Zhang, *Nano Lett.* **2015**, 15, 4440.
- [36] A. Aribia, J. Sastre, X. Chen, M. H. Futscher, M. Rumpel, A. Priebe, M. Döbeli, N. Osenciat, A. N. Tiwari, Y. E. Romanyuk, *Adv. Energy Mater.* **2022**, 12, 4.
- [37] J. Asenbauer, T. Eisenmann, M. Kuenzel, A. Kazzazi, Z. Chen, D. Bresser, *Sustainable Energy Fuels* **2020**, 4, 5387.
- [38] J.-H. Kuo, C.-C. Li, *J. Electrochem. Soc.* **2020**, 167, 100504.
- [39] S. Pedaballi, C. C. Li, *J. Power Sources* **2020**, 472, 228552.
- [40] M. Wood, J. Li, R. E. Ruther, Z. Du, E. C. Self, H. M. Meyer, C. Daniel, I. Belharouak, D. L. Wood, *Energy Storage Mater.* **2020**, 24, 188.
- [41] R. Sahore, M. Wood, A. Kukay, Z. Du, K. M. Livingston, D. L. Wood, J. Li, *J. Electrochem. Soc.* **2022**, 169, 040567.
- [42] R. Shunmugasundaram, R. Senthil Arumugam, P. Benedek, M. Yarema, P. Baade, V. Wood, *J. Electrochem. Soc.* **2022**, 169, 060504.
- [43] L. Neidhart, K. Fröhlich, N. Eshraghi, D. Cupid, F. Winter, M. Jahn, *Nanomaterials* **2022**, 12, 317.
- [44] S. Radloff, R.-G. Scurtu, M. Hölzle, M. Wohlfahrt-Mehrens, *J. Electrochem. Soc.* **2022**, 169, 040514.
- [45] P. P. Wang, C. Y. Xu, W. Da Li, L. Wang, L. Zhen, *Electrochim. Acta* **2015**, 169, 440.
- [46] N. Loeffler, G. T. Kim, F. Mueller, T. Diemant, J. K. Kim, R. J. Behm, S. Passerini, *ChemSusChem* **2016**, 9, 1112.